

Edge dislocation core structures in FCC metals determined from ab initio calculations combined with the improved Peierls-Nabarro equation *

Rui Wang,[†] Shaofeng Wang, Xiaozhi Wu

Institute for Structure and Function and Department of Physics, Chongqing University, Chongqing 400044, P. R. China

Abstract We have employed the improved Peierls-Nabarro (P-N) equation to study the properties of $1/2\langle 110 \rangle$ edge dislocation in $\{111\}$ plane in FCC metals Al, Cu, Ir, Pd, and Pt. The generalized-stacking-fault energy (GSFE) surface entering the equation is calculated by using first-principles density functional theory (DFT). The accuracy of the method has been tested by calculating values for various stacking fault energies which favorably compare with the previous theoretical and experimental results. The core structures, including the core widths both of the edge and screw components, dissociation behavior for edge dislocations have been investigated. The dissociated distance between two partials for Al in our calculation agrees well with the values obtained from the numeric simulation with DFT and molecular dynamics simulation, as well as experiment. Our calculations show that it is preferred to create partial dislocation in Cu, and to be easily observed full dislocation in Al, Ir, Pd, and especially Pt.

PACS: 61.72.Bb; 71.15.Mb.

Keywords: FCC Metals; Ab initio calculations; Generalized-stacking-fault energy (GSFE); Dislocation properties; Improved Peierls-Nabarro equation.

1 Introduction

It is widely accepted that the dislocations have a direct influence on the deformation mechanism of materials [1], and there has been a great deal of interest in describing accurately the dislocation core structure on an atomic scale because of its important role in many phenomena of crystal plasticity [2, 3]. In FCC metals dislocations can reduce elastic energy by dissociating into Shockley partial dislocations connected by a stacking fault [1]. But as the core regions of two partials overlap, whether the partials can be observed has not been governed by the stacking fault energy but also generally by atomic interactions. The dislocations in Al have always been focused on in the past twenty years [4, 5, 6, 7, 8, 9, 10, 11, 12, 13]. The accurate prediction of the atomic-scale core geometries for dislocations in Al is needed to inform higher-length scale models of plasticity in Al alloys,

*Project supported by the National Natural Science Foundation of China (11074313) and Project No. CDJXS11102211 supported by the Fundamental Research Funds for the Central Universities.

[†]Corresponding author. E-mail: rcwang@cqu.edu.cn; tel: +86 13527528737

as well as as other FCC metals [4]. In addition, it is well known that the nature of slip cannot be described in terms of an absolute value of stacking fault energy and a correct interpretation requires the generalized-stacking-fault energy (GSFE) curve, involving both intrinsic (stable) and unstable stacking fault energies [14].

There are usually two types of theoretical approaches which have been employed to study the core properties of dislocations. The first method is based on direct atomistic simulations or first-principles calculations, and the second method is based on the the framework (Peierls-Nabarro) P-N model. Empirical interatomic potentials involve the fitting of parameters to a predetermined database and hence may not reliable in describing the core properties. On the other hand, first-principles calculations, though considerably more accurate, are computationally expensive for studies of dislocation properties. The P-N model, in which the discreteness of crystal is neglected, is essentially a continuum treatment, but the dislocation core, the region of inelastic displacement, is given an approximate atomistic description. In addition, the partials in FCC metals are mixed dislocations with both edge and screw components [4]. Schoeck and Mryasov et al adopted the generalized 2D P-N model to consideration the two-component displacement field of dissociated dislocation [8, 15, 16], but discreteness of crystals is neglected. Recently, the 2D improved P-N dislocation equation taken into account the discreteness of crystals based on the lattice dynamics and the symmetry principle has been obtained [17, 18]. Both for the P-N model and improved P-N equation [18], the forces in the dislocation core, where the atomic atomic-scale discreteness really counts, are currently approximated with the GSFE surface (γ -surface) [3, 13, 19, 20]. The GSFE surface is the interplanar potential energy, which can currently be calculated accurately from ab initio calculations, for sliding one half of a crystal over the other half.

In this paper, we carry out first principles calculations on the GSFE surfaces (γ -surface) for FCC metals Cu, Al, Ir, Pd, and Pt. The γ -surfaces are applied in the improved P-N equation to the edge dislocations. The accuracy of the method has been tested by calculating values for various stacking fault energies which favorably compare with the previous theoretical and experimental results. Dislocation structures are calculated, including the core widths and dissociated distance between two partials. This paper is organized as follows. In section 2, we carry out the first principles calculation of GSFE surface on (111) plane in FCC metals Cu, Al, Ir, Pd, and Pt. In section 3, the core structure of dissociated dislocation is obtained from the improved P-N equation with variational method, and dislocation properties have also been discussed.

2 First principles calculations of generalized-stacking-fault-energy surface

2.1. Computational Methodology

In the present study total-energy calculations based on the density functional theory (DFT) embodied in the Vienna ab simulation package (VASP) [21, 22, 23] is employed. The Perdew-Burke-Ernzerhof (PBE)

[24, 25] exchange-correlation functional for the generalized-gradient-approximation(GGA) is used. A plane-wave basis set is employed within the framework of the projector augmented wave (PAW) method [26, 27]. On the basis of our tests, we have chosen the plane-wave energy cutoff of 500 eV for all calculated metals. An initial calculation is undertaken to determine the optimum lattice constants as well as the elastic constants. For the first-Brillouin-zone integrals, reciprocal space is represented by Monkhorst-Pack-special k-point scheme [28] with $15 \times 15 \times 15$ grid meshes for these initial calculations, while the generalized-stacking-fault energy (GSFE) calculations employ $21 \times 21 \times 3$ grid meshes for our calculated FCC metals Cu, Al, Ir, Pd, and Pt. The equilibrium theoretical lattice structures are determined by minimizing the Hellmann-Feynman force on the atoms and the stress on the unit cell. The convergence of energy and force are set to $1.0 \times 10^{-6} eV$ and $1.0 \times 10^{-4} eV/\text{\AA}$, respectively. In Table 1, we give the all equilibrium lattice constants and elastic modulus for all studied FCC metals in our calculation, and it is shown that the results agree well with the experiment values [29, 30].

2.1. The generalized-stacking-fault energy surfaces

In the present study, we calculate the GSFE surfaces in the closed-packed (111) surface which is the trigonal lattice, since the slip between the closed-packed surfaces is most easily for FCC metals. The ideal FCC structures have the configuration $\cdots ABCABC \cdots$ stacking sequence of the atomic planes. To simulate the block shearing process we use a slab consisting of twelve atomic layers in the $\langle 111 \rangle$ direction. Between periodically repeated slab the vacuum space of 15\AA normal to (111) plane is chosen to avoid interactions between two slabs. The stacking-fault energies (SFEs) for the slab consisting of twelve and fourteen atomic layers are reasonably close. In addition, we find that the fluctuations of calculated results for vacuum gap of 15\AA and 18\AA are less than 1.0%. So, the adequate convergence with respect to the supercell size consisting of twelve atomic-layers thick slab and vacuum gap of 15\AA is indicated. The slab calculations is appropriate since the fault interactions are short ranged [13]. Comparison with a six atomic-layers thick slab calculations of intrinsic-stacking-fault (ISF) by Hartford et al [13], our twelve atomic-layers thick slab calculation is more accurate, but with great computational consumption.

The SFEs are determined as a difference of total energies for two sides of the slab, in which there are six atomic layers for below and above, designed to simulate faults with vectors $\mathbf{u} = 0$ and $\mathbf{u} \neq 0$. The stacking-fault (SF) vector \mathbf{u} , which is a two-dimension (2D) vector (u_x, u_y) , is the displacement of the upper half-crystal relative to the one below. The ISF configuration corresponds to a slip of $\frac{a}{\sqrt{6}}$ in the $\langle 112 \rangle$ direction, resulting in the SF vector $\mathbf{u} = \frac{a}{\sqrt{6}}(\frac{\sqrt{3}}{2}, \frac{1}{2})$ (where a is the lattice constant). The unstable stacking-fault energy (USFE) γ_{USF} corresponds to the lowest energy barrier that needs to be crossed for the slip from the ideal configuration to the ISF configuration in the $\langle 112 \rangle$ direction. In order to obtain the correct SFEs, structural optimizations must

be considered in this study. The relaxations perpendicular to the (111) plane are carried out by a combined optimization of supercell volume and atomic coordinates in shifted configuration.

To obtain the GSFE surfaces of FCC metals, we have calculated SFEs for the slips along the $\langle 112 \rangle$ and $\langle 110 \rangle$ directions, respectively. Taking Al as an example, the fitted GSFE surface is shown in Fig. 1, while the GSFE surfaces for other FCC metals has the similar shapes. The first energy maximum encountered along the $\langle 112 \rangle$ direction is the USFE γ_{USF} , which represents the lowest energy barrier for dislocation nucleation[?]; the first energy minimum value at $1/6\langle 112 \rangle$ ($a/\sqrt{6}$) corresponds to the ISF configuration, where a full dislocation dissociates into a pair of Shockley partials. The projection of the GSFE surface on the $\langle 110 \rangle$ direction are symmetric with respect to the slip displacement of $\sqrt{2}a/4$. In Fig. 2, we show the projection of the GSF energy surface on the $\langle 112 \rangle$ (Fig. 3(a)) and $\langle 110 \rangle$ (Fig. 3(b)) directions. The values of unstable stacking-fault (SF) energy along the $\langle 110 \rangle$ direction are found to be larger than one along the $\langle 112 \rangle$ direction. The energy values of the various stacking faults obtained from the DFT calculations are summarized in Table 2. We also compare our results with the previous theoretical results [13, 31, 32] and experimental results [1, 33, 34]. The calculated results of ISF energies (ISFEs) γ_{ISF} are in good agreement with the experimental values. Comparison with the results obtained from the EAM (embedded atom method) [31] or MEAM (modified EAM)[32] by Zhang et al, our results agree better with the experimental results. Our results for Al and Pd are also in consistent with the results obtained from Hartford et al [13] by first-principles calculations. The value of γ_I for Pt is 282mJ/m² which is in better agreement with the experimental value 322mJ/m² than the results 111mJ/m² obtained from MEAM [32].

The GSFE surface $\gamma(\mathbf{u})$ satisfies the translational symmetry,

$$\gamma(\mathbf{R} + \mathbf{u}) = \gamma(\mathbf{u}), \quad (1)$$

where \mathbf{R} is the lattice vector. The GSFE surface can be represented with the aid of reciprocal lattice by a 2D Fourier series which reflects the full symmetry of the (111) plane,

$$\gamma(\mathbf{u}) = \sum_{\mathbf{G}} \gamma_{\mathbf{G}} e^{i\mathbf{G} \cdot \mathbf{u}} \quad (2)$$

where \mathbf{G} is the reciprocal lattice vector. While the nearest neighbor approximation in reciprocal lattice space is taken into account

$$\begin{aligned} \gamma(u^x, u^y) = & \gamma_0 + \gamma_1 \left\{ \cos\left(\frac{4\pi u^y}{\sqrt{3}a}\right) + \cos\left(\frac{2\pi u^x}{a} + \frac{2\pi u^y}{\sqrt{3}a}\right) + \cos\left(\frac{2\pi u^x}{a} - \frac{2\pi u^y}{\sqrt{3}a}\right) \right\} \\ & + \gamma_2 \left\{ \sin\left(\frac{4\pi u^y}{\sqrt{3}a}\right) - \sin\left(\frac{2\pi u^x}{a} + \frac{2\pi u^y}{\sqrt{3}a}\right) + \sin\left(\frac{2\pi u^x}{a} - \frac{2\pi u^y}{\sqrt{3}a}\right) \right\} \end{aligned} \quad (3)$$

The coefficients γ_0 , γ_1 and γ_2 can be determined by the fitting to the GSFE surface that can be obtained by our first-principles calculations. γ_0 represents the ground state energy, which does not influence the shape of

GSFE surface and can be chosen to zero, so only γ_1 and γ_2 need to be fixed. We also list the fitted parameters γ_1 and γ_2 of Eq. (3) for all calculated FCC metals in Table 2. Eq. (3) is accurate to describe translational and reflection symmetry of the GSFE surface on (111) plane in FCC metals, and facilitates the computation of dislocation properties.

3 The dissociation of dislocation and the governing equation

3.1. The improved Peierls-Nabarro dislocation equation

In the (111) plane of FCC metals, the primary slip system is $\langle 112 \rangle (111)$, so dislocations with Burgers' vector $\frac{1}{2}\langle 110 \rangle$ will energetically favorable dissociate into two Shockley partials connected by a stacking-fault (SF) ribbon according to Frank's rule [1]. The dissociation process is described by the following reaction



The dissociation can be understood from the GSFE surfaces for slip plane (111). Fig.2 shows that the lowest energy path happens to be along the $\langle 112 \rangle$ direction, and perfect dislocations (Burgers' vector $\mathbf{b} = \frac{1}{2}[\bar{1}10]$) is likely to dissociate into partial dislocations (Burgers' vectors are $\mathbf{b}_1 = \frac{1}{6}[\bar{1}12]$ and $\mathbf{b}_2 = \frac{1}{6}[\bar{1}\bar{1}\bar{2}]$) due to the lower energy barrier. The two partial dislocations are 60° fractional dislocations viz. the included angle between the dislocation line and the Burgers vector is 60° . The magnitude of the total Burgers vector is $b = \sqrt{a}/2$ and a is the lattice constant for FCC metal. The Burgers vectors of the two partial dislocations have magnitudes $b_1 = b_2 = \sqrt{3}b/3$. Hereafter, let the dislocation lines parallel to the y-axis ($[11\bar{2}]$ direction) and perpendicular to the total Burgers vector of edge dislocation ($[\bar{1}10]$ direction). The x-component and y-component respectively represent the edge component and screw component of partial dislocations for dissociation from edge dislocation.

The 2D dislocation equation for straight dislocations that describe the balance of atoms on the border based on the lattice dynamics and the symmetry principle takes the following form [18]

$$\begin{aligned} -\frac{\beta_e}{2} \frac{d^2 u^x}{dx^2} - \frac{K_e}{2\pi} \int_{-\infty}^{+\infty} \frac{dx'}{x' - x} \left(\frac{du^x}{dx} \right) \Big|_{x=x'} &= f^x(u^x, u^y), \\ -\frac{\beta_s}{2} \frac{d^2 u^y}{dx^2} - \frac{K_s}{2\pi} \int_{-\infty}^{+\infty} \frac{dx'}{x' - x} \left(\frac{du^y}{dx} \right) \Big|_{x=x'} &= f^y(u^x, u^y), \end{aligned} \quad (5)$$

where K_e and K_s are the energy factors of the edge and screw dislocations, u^x and u^y are the edge and screw components of displacements. For the isotropic solid, $K_e = \mu\sigma/(1-\nu)$ and $K_s = \mu\sigma$, with μ being shear modulus and ν Poisson's ratio, σ is the area of the primitive cell of the misfit plane. The shear modulus and the Poisson's ratio can be expressed as the second-order elastic constants c_{ij} , i.e., $\mu = (c_{11} - c_{12})/2$ and $\nu = c_{12}/(c_{11} + c_{12})$ (the values as shown in Table 1). The coefficients of the second-order derivations β_e and β_s relate with the acoustic

phonon velocity and the lattice geometry structure

$$\beta_e = \frac{3}{4}\Omega\mu\left(\frac{2-2\nu}{1-2\nu} - \tan^2\theta\cos^2\phi\right), \quad (6)$$

$$\beta_s = \frac{3}{4}\Omega\mu(1 - \tan^2\theta\sin^2\phi), \quad (7)$$

where θ and ϕ are the orientation angles of the relative position of a pair of neighbor atoms in the intrinsic frame with the axes given by the polarization directions, and $\theta = \pi/4$ and $\phi = \pi/6$ for FCC crystals, Ω is the volume of the primitive cell. Comparing with the generalized 2D P-N equation in P-N model, there are two extra second-order derivations that represent the discreteness effect of crystal in the new equation. From exactly solvable models [17, 18] in which discreteness of a lattice can be fully considered, one clearly sees the discreteness correction appearing in terms of the second-differential of the displacement. Physically, the integro term in Eq. (5) represents a long range interaction which is inversely proportional to the distance, the differential term describes short range interaction which results from the interaction among the atoms on the surface plane. While β_e and β_s are taken to be zero namely the discreteness effect is neglected the generalized 2D P-N equation can be obtained [16].

3.2. The core properties of dissociated dislocation with variational method

The dislocation solution of 2D dislocation equation is unknown. In this paper, the variational method is applied for the 2D dislocation equation [17, 35]. It can be straightforwardly verified that the variational functional of the 2D dislocation equation takes the following form

$$\begin{aligned} J = & -\frac{\beta_e}{4} \int_{-\infty}^{+\infty} \left(\frac{du^x}{dx}\right)^2 dx - \frac{K_e}{4\pi} \int_{-\infty}^{+\infty} \int_{-\infty}^{+\infty} \frac{du^x}{dx} \frac{du^x}{dx} \Big|_{x=x'} \ln \left| \frac{x-x'}{d} \right| dx dx' \\ & -\frac{\beta_s}{4} \int_{-\infty}^{+\infty} \left(\frac{du^y}{dx}\right)^2 dx - \frac{K_s}{4\pi} \int_{-\infty}^{+\infty} \int_{-\infty}^{+\infty} \frac{du^y}{dx} \frac{du^y}{dx} \Big|_{x=x'} \ln \left| \frac{x-x'}{d} \right| dx dx' \\ & + \int_{-\infty}^{+\infty} \gamma(u^x, u^y) dx, \end{aligned} \quad (8)$$

where d is the distance of the nearest atoms in the misfit plane.

In order to obtain the structure of dissociated dislocation, we represent each of the two partials by two closely spaced Peierls dislocations (of arctan-type) that can assure the correct asymptotic behavior. Thus, trial dislocation solution for dissociated dislocation can be written as

$$\begin{aligned} u^x &= \frac{b}{2\pi} \left\{ \arctan\left(\frac{x+d_{eq}/2}{\zeta_e}\right) + \arctan\left(\frac{x-d_{eq}/2}{\zeta_e}\right) \right\} + \frac{b}{2}, \\ u^y &= \frac{\sqrt{3}b}{6\pi} \left\{ \arctan\left(\frac{x+d_{eq}/2}{\zeta_s}\right) - \arctan\left(\frac{x-d_{eq}/2}{\zeta_s}\right) \right\}, \end{aligned} \quad (9)$$

where d_{eq} is the equilibrium separation of two partial dislocations and $\pm d_{eq}/2$ are the positions of the two partials, ζ_e and ζ_s represent the core width of the edge and screw components respectively. The relation between

the edge and screw components of the relative displacement determines the dissociation path in the glide plane. Generally, the width of edge component ζ_e is not equal to that of screw component ζ_s and the dissociation path deviates from the crystallographic Burgers vector [16]. Thus, the dissociated dislocations cannot be dealt with 1D dislocation equation.

Substituting the trial solution into the variational functional Eq.(8), the total variational functional J is as a function of d_{eq} , ζ_e and ζ_s . The separation and the width of edge and screw components can be determined by solving the following equations

$$\frac{\partial J}{\partial d_{eq}} = 0, \quad (10)$$

$$\frac{\partial J}{\partial \zeta_e} = 0, \quad (11)$$

$$\frac{\partial J}{\partial \zeta_s} = 0. \quad (12)$$

After a tedious although straightforward algebra one can obtain that the variational parameters of the trial dislocation solutions Eqs.(9) for all our calculated FCC metals. Table 3 gives observed and calculated dissociated distances for the Al edge-character partial dislocation, in comparison with the wide range of previous results based on P-N model, atomistic simulations and density-functional theory (DFT). The partial separation distance in our results is $3.6b$ (where b is length of the total Burgers' vector), which is in good agreement with the experiment value $2.8b$ obtained from weak-beam transmission electron microscopy [5] and the simulated value $2.4b \sim 3.4b$ from DFT method in which the periodic supercell uses 552 atoms in a large radius cylindrical slab surrounded by vacuum [4], as well as the value $3.2b$ obtained from the molecular dynamics simulation with the glue potential [10]. An earlier DFT calculation, which employed the quasi-continuum (QC) DFT method, where a small first principles cell containing the dislocation is embedded in the strain field produced by atoms interacting through an interatomic force law based on the embedded atom method (EAM), gives a smaller dissociated distance $2.0b$ [7]. The difference of the QC-DFT-EAM calculation most likely stems from the small (84 atoms) supercell used for the first-principles calculations. The P-N model, which is a semidiscrete model, is essentially a continuum treatment. But the atomic-scale discreteness of crystals really matters in the region of partial dislocation core, so P-N models [7, 8] are not well suited for describing details of the strain field in partial core. Different implementations of the P-N model predict different dissociated distances, though both are based on first-principles calculations of the GSFE surface. Several atomistic simulations for edge dislocation in Al have obtained different results for the dissociated distance between two partials, ranging from $1.7b \sim 5.6b$ [10, 11, 12]; this variation is possible the result of different treatments for the boundary conditions [4]. In our calculation, the GSFE surface is calculated from first-principle calculations accurately and the 2D improved P-N equation Eqs.(5) fully includes the discreteness effect of crystal, so our method is appropriate for dealing

with the Shockley partials which are the mixture dislocations including edge component and screw component. The disregistry and the dislocation density which is defined as $\rho = du/dx$ for Al, determined from our first principles calculations combined with the improved P-N equation, are shown in Fig. 3 (a) and (b), respectively. It is worth noting that the maximum value of relative displacements along y-axis u_y for Al is $0.13b$, and is much smaller than the projection on the y-axis of the Burgers' vector of the partial $\frac{1}{6}\langle 112 \rangle = 0.29b$ (the black dot in Fig.3(a)). This means that the area within two partials is not a pure stacking fault ribbon, where the core regions of the two partials overlap and the displacement of y-component annihilate with each other due to the opposite direction [8, 37]. The structure of dislocations in Al cannot be dealt with the 1D model due to the strong overlap of two partials as illustrated in Fig.3(b). The two partial dislocations can not be identified due to the large overlap that is consistent with the experiment and the first principle simulation [4].

In this work, the core structures of edge dislocation in other FCC metals Cu, Ir, Pd, and Pt have also been calculated by using first principles calculations GSFE surfaces based on the improved P-N equation. The core widths both of the edge and screw components and the dissociated distances are listed in Table 4, and the disregistry and the dislocation density for Cu, Ir, Pd, and Pt are shown in Fig.4, Fig. 5, Fig.6, and Fig.7, respectively. We also listed the results obtained from the P-N model in which the second-derivative term is neglected in Table 4. One can see that the discrete effects always increase the widths both for edge and screw components. Physically, the improved P-N equation Eq.(5) is more functional to determine the structures of dislocation than the classical P-N equation [18], but for the calculated FCC metals we regret not being able to find any experimental data which would clearly demonstrate that the results with second-derivative term are more superior than those without second-derivative term. We cannot be sure that which model is a better one at the present level of knowledge. However, we believe the new experimental results will clarify this question mark.

It has been known that the deformation mechanism cannot be explained by the absolute value of ISFE γ_{ISF} alone and the entire behavior has to be understood in terms of the ratio $\gamma_{USF}/\gamma_{ISF}$ along $\langle 112 \rangle$ [14], so we also list the ratios of $\gamma_{USF}/\gamma_{ISF}$ in Table 4. When this ratio is low, then the energy barrier that has to be overcome for creating a trailing partial is very low and therefore it will be possible to observe the full dislocation. Pt has the lowest ratio $\gamma_{USF}/\gamma_{ISF}$ value 1.10 in our calculation, so the overlap of two partials is so strong that one cannot distinguish them though dissociation behavior exists. In Fig .7, we can see that the maximum value of u_y for Pt is $0.11b$ and two-peak of the dislocation density for edge component ρ_x vanishes. But when this ratio is large, the energy increase necessary for nucleating the trailing partial substantial, which is in the case of Cu with the large ratio $\gamma_{USF}/\gamma_{ISF}$ value 4.07. In Fig. 4, we can indicate that the overlap of two partials is weak in Cu. It has verified in simulations (Ref[38]) extended partial dislocations in Cu have been observed as the predominant

deformation mechanism at nanocrystalline grains. It is worth noting that though the dissociated distance $5.5b$ for Pt is larger than that $5.4b$ for Pd, the core width of Pt is larger than that of Pd. This explains why Fig. 6 for Pd shows two-peak of ρ_x but Fig .7 for Pt does not. Our detailed calculations demonstrate that whether full dislocations or Shockley partials will easily be observed in FCC lattice must be understood in terms of the ratio $\gamma_{\text{USF}}/\gamma_{\text{ISF}}$.

4 conclusion

In conclusion, we have performed first-principles calculations to obtain the GSFE surface for the $\{111\}$ glide plane in FCC metals Cu, Al, Ir, Pd, and Pt. The accuracy of the method have been tested by calculating values for various stacking fault energies which favorably compare with the previous theoretical and experimental results. From these calculations, we extract the core properties for the edge dislocation of dissociation into partials, using the improved P-N equation which includes the discreteness effect of crystal. The Ritz variational method is presented to solve the dislocation equation and the trial solution is constituted by two arctan-type functions which represents the dislocation dissociating into two partials. The core structures, including the core widths both of the edge and screw components, dissociation behavior for edge dislocations have been investigated. The dissociated distance between two partials for Al in our calculation agrees well with the values obtained from the numeric simulation with DFT and MD methods, as well as experiment. Our detailed calculations demonstrate that whether full dislocations or Shockley partials will easily be observed in FCC lattice must be understood in terms of the ratio $\gamma_{\text{USF}}/\gamma_{\text{ISF}}$, and show that it is preferred to create partial dislocation in Cu, and to be easily observed full dislocation in Al, Ir, Pd, and especially Pt

References

- [1] J.P. Hirth and J. Lothe, Theory of dislocations, New York: John Wiley, 2nd ed., 1982, 835.
- [2] M. S. Duesbery and G. Y. Richardson, CRC Crit. Rev. Solid State Mater. Sci. 17 (1991) 1.
- [3] V. Vitek, Prog. Mater. Sci. 36 (1992) 1.
- [4] C. Woodward, D. R. Trinkle, L. G. Hector, J. Olmsted, and D. L. Olmsted, Phys. Rev. Lett. 100 (2008) 045507.
- [5] W. Höllerbauer and H. P. Karnthaler, Beitr. Elektronenmikroskop. Direktabb. Oberfl. 14 (1981) 361.

- [6] G. Lu, E. B. Tadmor, and E. Kaxiras, *Phys. Rev. B* 73 (2006) 024108.
- [7] G. Lu, N. Kioussis, V.V. Bulatov, and E. Kaxiras, *Mater. Sci. Eng. A* 309C310 (2001) 142.
- [8] G. Schoeck, *Mater. Sci. Eng. A* 333 (2002) 390.
- [9] R. Wang and Q. F. Fang, *J. Alloys Comp.* 310 (2000) 80-84.
- [10] D. L. Olmsted and R. D. Phillips (to be published).
- [11] S. G. Srinivasan, X. Z. Liao, M. I. Baskes, R. J. McCabe, Y. H. Zhao, and Y. T. Zhu, *Phys. Rev. Lett.* 94 (2005)125502.
- [12] Y. Mishin, D. Farkas, M. J. Mehl, and D. A. Papaconstantopoulos, *Phys. Rev. B* 59 (1999) 3393.
- [13] J. Hartford, B. Sydow and G. Wahnstrom et al., *Phys. Rev. B*, 58 (1998) 2487.
- [14] H. V. Swygenhoven, P. M. Derlet, A. G. Frøseth, *Nature Mater.* 3 (2004) 399.
- [15] G. Schoeck, *Mater. Sci. Eng. A* 400 (2005) 7.
- [16] O.N. Mryasov, Y.N. Gornostyrev and A.J. Freeman, *Phys. Rev. B*, 58 (1998) 11927.
- [17] S.F. Wang, *Phys. Rev. B* 65 (2002) 094111.
- [18] S. F. Wang, *J. Phys. A: Math. Theor.* 42 (2009) 025208.
- [19] V. Vitek, *Phil. Mag.* 18 (1968) 773.
- [20] V. Vitek, *Cryst. Lattice Defects* 5 (1974) 1.
- [21] G. Kresse and J. Hafner, *Phys. Rev. B* 48 (1993) 3115.
- [22] G. Kresse and J. Furthmüller, *Comput. Mater. Sci.* 6 (1996)15.
- [23] G. Kresse and J. Furthmüller, *Phys. Rev. B* 54 (1996)11169.
- [24] J. P. Perdew, K. Burke, and M. Ernzerhof. *Phys. Rev. Lett.* 77 (1996) 3865.
- [25] J. P. Perdew, K. Burke, and M. Ernzerhof, *Phys. Rev. Lett.* 78 (1996) 1396.
- [26] P. E. Blöchl, *Phys. Rev. B* 50(1994) 17953.
- [27] G. Kresse and D. Joubert, *Phys. Rev. B* 59 (1999) 1758.
- [28] H. J. Monkhorst and J. D. Pack, *Phys. Rev. B* 13 (1976) 5188.
- [29] American Institute of Physics Handbook, 3rd ed. (McGraw-Hill, New York, 1970).
- [30] G. Simmons and H. Wang, *Single Crystal Elastic Constants and Calculated Aggregate Properties: A Handbook*, 2nd ed. (MIT Press, Cambridge, MA, 1971).
- [31] J. M. Zhang, X. J. Wu, Y. J. Huang, K. W. Xu, *Acta. Phys. Sin.* 55 (2006) 0394.
- [32] X. M. Wei, J. M. Zhang, K. W. Xu, *Appl. Surf. Sci.* 254 (2007) 1489.
- [33] M. Grujicic, P. Dong, *Mat. Sci. Eng. A* 201 (1995) 194.
- [34] P. R. Thorntor, P. B. Hirsch, *Phil. Mag.* 3 (1958) 738.
- [35] S.F. Wang, X.Z. Wu and Y.F. Wang, *Phys. Scr.*, 76 (2007) 593.
- [36] G. V. Sin'ko and N. A. Smirnov, *Phys. Rev. B*, 80 (2009) 104113.
- [37] Q. F. Fang, and R. Wang, *Phys. Rev. B*, 62 (2000) 9317.
- [38] J. Schiøtz, K. W. Jacobsen, *Science* 301 (2003) 1357.

Table 1 The calculated equilibrium lattice parameters a [Å] and elastic constants [GPa], comparison with the experimental and previous calculated results.

	a	c_{11}	c_{12}	c_{44}	μ	ν
Al	4.05, 4.05 ^a	112.3, 114.3 ^b	60.7, 61.3 ^b	30.2, 31.6 ^b	25.8, 26.3 ^b	0.350, 0.349 ^b
Cu	3.64, 3.62 ^a	175.3, 176.2 ^b	124.4, 124.9 ^b	80.9, 81.8 ^b	25.5, 25.7 ^b	0.415, 0.415 ^b
Ir	3.88, 3.84 ^a	579.6, 582.3 ^b	240.8, 241.3 ^b	261.2, 262.0 ^b	167.9, 170.5 ^b	0.294, 0.293 ^b
Pd	3.96, 3.89 ^a	232.1, 234.1 ^b	175.2, 176.1 ^b	70.5, 71.2 ^b	28.5, 29.0 ^b	0.430, 0.420 ^b
Pt	3.99, 3.92 ^a	356.8, 358.0 ^b	252.2, 253.6 ^b	76.3, 77.4 ^b	52.3, 52.2 ^b	0.414, 0.415 ^b

^aReference[29]

^bReference[30]

Table 2 The various stacking-fault energies on (111) plane for FCC metals. The experimental and the other calculated results are also listed. All values are in units of mJ/m².

	Cu	Al	Ir	Pd	Pt
γ_1	-160	-158	-615	-167	-171
γ_2	-260	-213	-928	-243	-188
γ_{ISF}	43	158	359	122	282
γ_{ISF}^a	75	146	41	244	356
γ_{ISF}^b	43	150	-	101	111
γ_{ISF}^c	51	153	-	186	-
γ_{ISF}^d	40, 45, 169	166	300	180	322
γ_{USF} along $\langle 112 \rangle$	175	225	753	215	311
γ_{USF} along $\langle 110 \rangle$	638	633	2462	668	685

^aReference[31], by EAM calculations

^bReference[32], by MEAM calculations;

^cReference[13], by first-principles calculations;

^dReference[1, 33, 34], by experiments.

Table 3 Shockley partial dissociated distance d_{eq} for $1/2\langle 110 \rangle$ edge dislocations in Al. Our calculated result is compared with the experimental results, the previous theoretical values including the Peierls-Nabarro methods and the numerical simulations. All data are in units of the length of Burgers vector $b = \sqrt{2}/2a$.

This work	^a Ref[5]	^b Ref[4]	^b Ref[6]	^c Ref[7]	^c Ref[8]	^d Ref[9]	^d Ref[10]	^d Ref[11]
3.6	2.8	2.5 ~ 3.4	2.0	1.2	2.6	3.2	5.1	5.6, 1.7 ~ 5.2

^a experiment from weak-beam transmission electron microscopy (WB-TEM)

^b obtained from density-functional theory (DFT);

^c obtained from Peierls-Nabarro model;

^d obtained from atomistic simulations

Table 4 The predicted core structures, including core widths both the edge and screw components, dissociated distance in FCC metals Cu, Al, Ir, Pd, and Pt are listed. For completeness, we also list the results obtained from the P-N model in which the second-derivative term is neglected. For discussion, we give the ratio $\gamma_{\text{USF}}/\gamma_{\text{ISF}}$ values along the $\langle 112 \rangle$ direction. The ratio of $\gamma_{\text{USF}}/\gamma_{\text{ISF}}$ is dimensionless, and ζ_e , ζ_s and d_{eq} are in units of the length of Burgers vector $b = \sqrt{2}/2a$.

	Cu	Al	Ir	Pd	Pt
ζ_e	2.6 ^a , 2.1 ^b	2.5 ^a , 2.0 ^b	3.5 ^a , 3.1 ^b	3.1 ^a , 2.4 ^b	4.8 ^a , 4.0 ^b
ζ_s	1.9 ^a , 1.5 ^b	2.1 ^a , 1.6 ^b	2.9 ^a , 2.5 ^b	2.4 ^a , 1.8 ^b	3.9 ^a , 3.0 ^b
d_{eq}	5.5 ^a , 3.7 ^b	3.6 ^a , 2.6 ^b	5.6 ^a , 4.6 ^b	5.4 ^a , 3.5 ^b	5.5 ^a , 4.0 ^b
$\gamma_{\text{USF}}/\gamma_{\text{ISF}}$	4.07	1.42	2.10	1.76	1.10

^a obtained from improved P-N equation (with second-derivative term)

^b obtained from P-N equation (without second-derivative term).

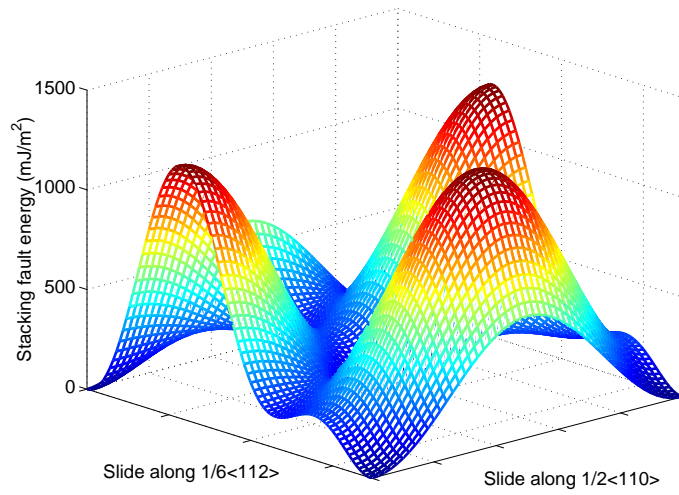


Fig. 1 The GSFE surface for displacements along a (111) plane in Al (the corners of the plane and its center correspond to the configurations of ideal Al lattice). The first energy maximum encountered along the $\langle 112 \rangle$ direction is the USFE; the first energy minimum value at $1/6\langle 112 \rangle$ corresponds to the ISF configuration. The projection of the GSFE surface along the $1/2\langle 110 \rangle$ is symmetric with respect to the slip displacement of $\sqrt{2}a/4$.

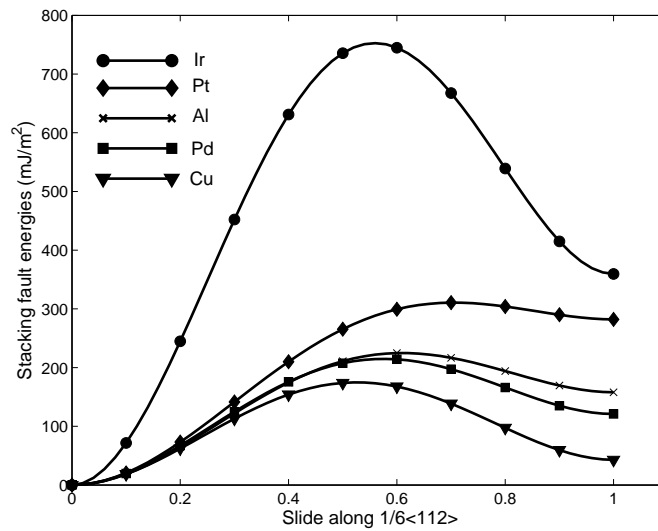


Fig. 2 Projection of the γ -surface in the $[11\bar{2}]$ directions on the (111) plane. There have been termed the intrinsic stacking fault (ISF) energies corresponding to the final positions and the unstable stacking fault (USF) energies corresponding to the maximum of the curves.

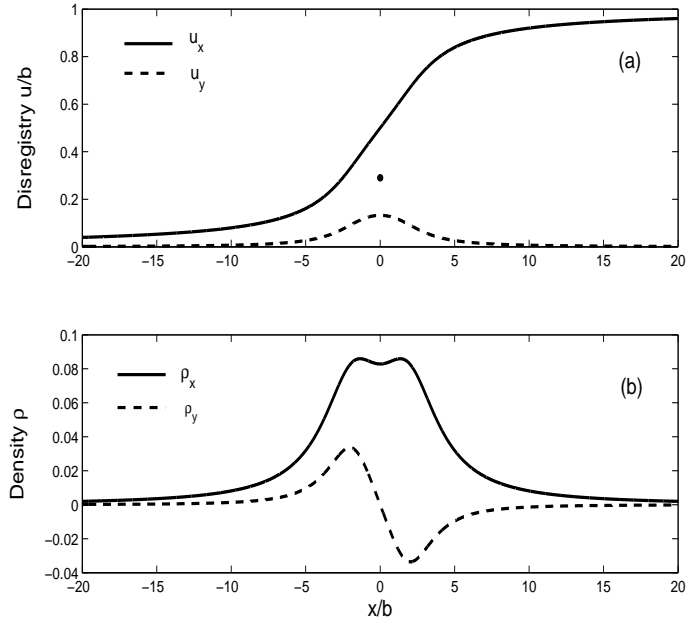


Fig. 3. Disregistry profile $u(x)$ (a) and dislocation density (b) for the edge dislocation in Al are obtained from our first-principles calculations combined with the improved P-N equation. The solid line and the dashed line represent the edge and screw components of displacements, respectively. The black dot marks the displacement of the screw component of the crystallographic Shockley partial dislocation, which is about $0.29b$. Here the maximum value of relative displacements of screw components of the partial dislocation is $0.13b$.

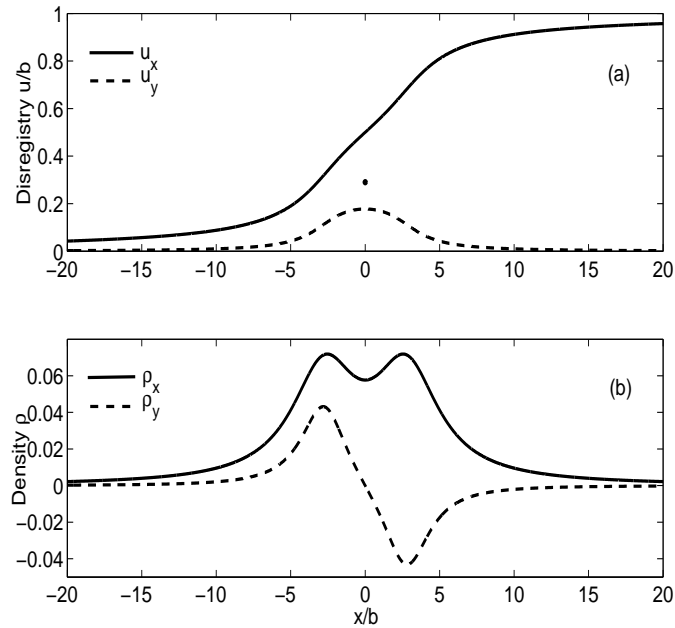


Fig. 4. Same as in Fig. 3, but for Cu. Here the maximum value of relative displacements of screw components of the partial dislocation is $0.20b$.

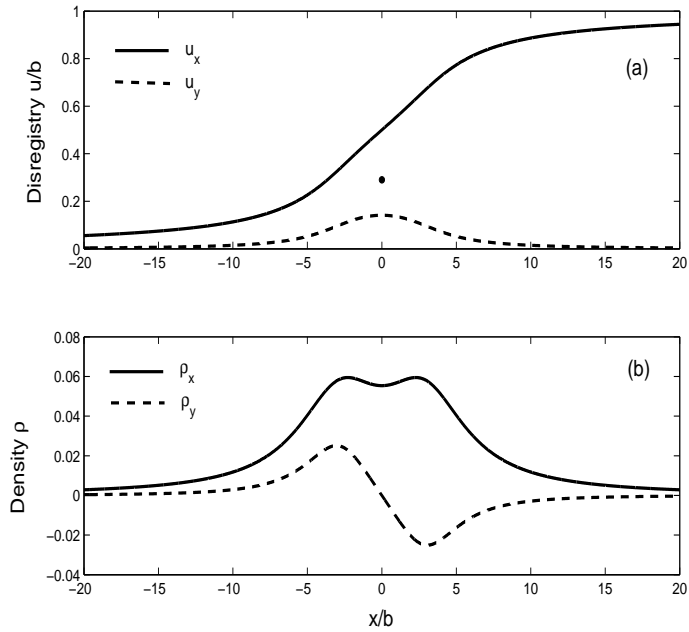


Fig. 5. Same as in Fig. 3, but for Ir. Here the maximum value of relative displacements of screw components of the partial dislocation is $0.15b$.

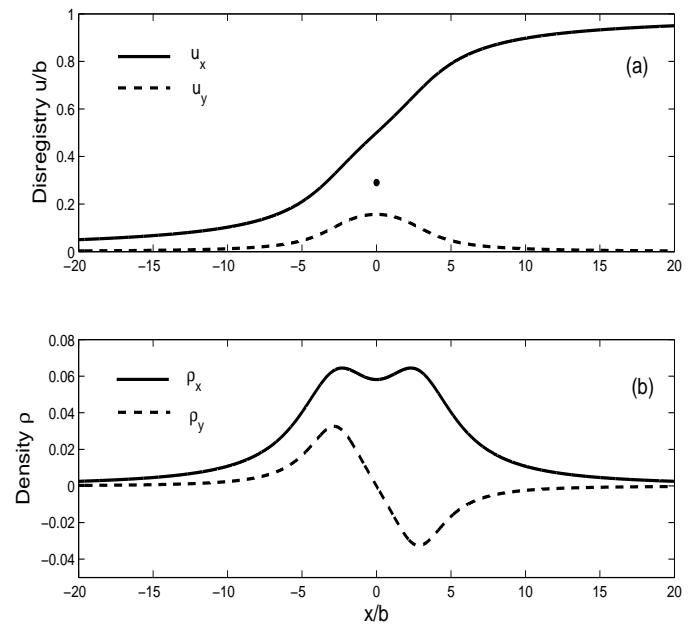


Fig. 6. Same as in Fig. 3, but for Pd. Here the maximum value of relative displacements of screw components of the partial dislocation is $0.15b$.

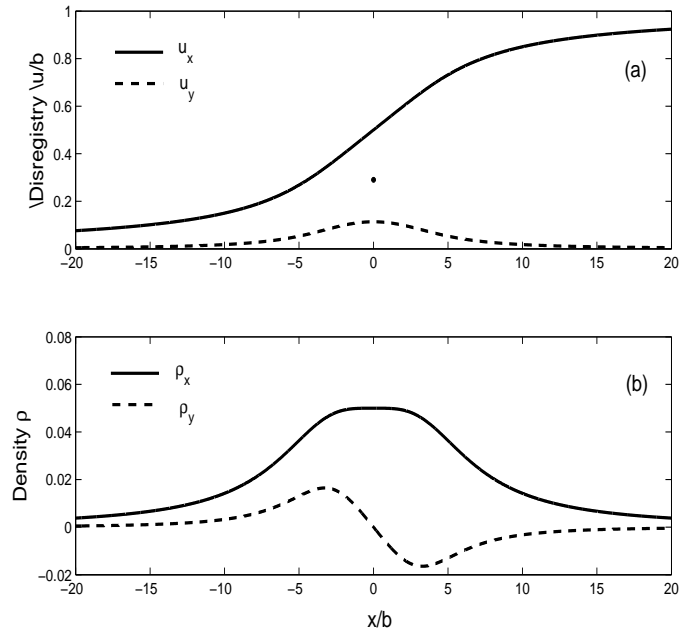


Fig. 7. Same as in Fig. 3, but for Pt. Here the maximum value of relative displacements of screw components of the partial dislocation is $0.11b$.